The Aminodiazonium Cation, $H_2N_3^+$ †

Karl O. Christe,*,[1] William W. Wilson,[1] David A. Dixon,[2] Saeed I. Khan,[3] Robert Bau,[4] Tobias Metzenthin,[4] and Roy Lu[4]

Contribution from Rocketdyne, A Division of Rockwell International Corporation, Canoga Park, California 91309, Central Research and Development Department, E. I. du Pont de Nemours and Company, Inc., Experimental Station, Wilmington, Delaware 19880-0328, J. D. McCullough X-ray Crystallography Laboratory, Department of Chemistry and Biochemistry, University of California, Los Angeles, California 90024, and Department of Chemistry, University of Southern California, Los Angeles, California 90089. *Received August 13, 1992*

Abstract: The $H_2N_3^+$ salts of SbF_6^-, AsF_6^-, and BF_4^- have been prepared and, for the first time, been isolated from HF solutions of HN_3 and the corresponding Lewis acids. They are hygroscopic white solids which are stable at room temperature. The crystal structure of $H_2N_3^+SbF_6^-$ was determined at 20 K. This compound crystallizes in the orthorhombic system, space group $Pmc2_1$, with two molecules in a unit cell of dimensions a = 5.794 (3) Å, b = 5.113 (2) Å, and c = 9.919 (5) Å with R = 0.015, R_w = 0.022, for 587 observed [$I > 3\sigma(I)$] reflections. In addition to two almost perfectly octahedral SbF_6^- anions, the unit cell contains two asymmetric $H_2N_3^+$ cations with N(1)-N(2) = 1.295 (5) Å, N(2)-N(3) = 1.101 (6) Å, and N(1)-N(2)-N(3) = 175.3 (5)° and both hydrogens bonded to the same nitrogen atom, N(1). The infrared and Raman spectra of these salts were also recorded. Local density functional calculations were carried out for $H_2N_3^+$ and isoelectronic H_2NCN and used for the assignment of the observed vibrational spectra and the determination of their force fields. The general agreement between the calculated and observed geometries and frequencies is very good. The results from the LDF calculations indicate that the $H_2\ddot{N}$ group in $H_2N_3^+$ is less pyramidal than that in H_2NCN and, therefore, possesses a lower inversion energy barrier.

Introduction

During our attempted fluorination of HN_3 in anhydrous HF solutions using either $XeF^+AsF_6^-$ or F_2 and the Lewis acids SbF_5, AsF_5, and BF_3, stable white solids were isolated which were identified as $H_2N_3^+$ salts of the corresponding Lewis acids. Relatively little had been known about salts derived from protonated hydrazoic acid. In 1966, Schmidt reported[5] the preparation of $H_2N_3^+SbCl_6^-$ from the reaction of HN_3 with $SbCl_5$ and HCl in CH_2Cl_2 at -78 °C. On the basis of the observation of an infrared band at 1522 cm^{-1}, which on deuteration was shifted to 1163 cm^{-1}, he proposed that $H_2N_3^+$ has the asymmetric aminodiazonium structure, $H_2N{-}N_2^+$, and not the symmetric diazenium structure, $[HN{=}N{=}NH]^+$. However, out of the nine fundamental vibrations expected for $H_2N{-}N_2^+$, only four were experimentally observed, and no explanation was offered for the absence of the other five bands. In 1983, Olah and co-workers studied the protonation of HN_3 in HF/SbF_5, HF/BF_3, and HSO_3F/SbF_5 solutions.[6] By ^1H and ^{15}N NMR spectroscopy, they unequivocally established that $H_2N_3^+$ has indeed the asymmetric aminodiazonium structure but did not isolate or further characterize these salts. On the basis of ab initio molecular orbital calculations at the 3-21G level of theory, they furthermore concluded that the aminodiazonium structure, $H_2N{-}N_2^+$, is favored by 49.8 kcal mol^{-1} over the symmetric diazenium structure, $[HN{=}N{=}NH]^+$ and that the optimized $H_2N{-}N_2^+$ structure has the following planar configuration of symmetry C_{2v}:

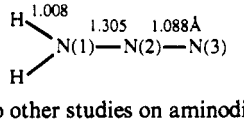

To our knowledge, no other studies on aminodiazonium salts have been published.

Experimental Section

Caution! Neat hydrazoic acid is shock sensitive, and proper safety precautions, such as working on a small scale and using safety shields, should be taken when handling the material.

Materials. HN_3 was prepared from NaN_3 and stearic acid at 110-130 °C.[7] HF (Matheson) was dried by storage over BiF_5.[8] AsF_5, SbF_5 (Ozark Mahoning), and BF_3 (Matheson) were purified by fractional condensation prior to use.

Apparatus. HN_3 was generated and handled on a Pyrex vacuum line equipped with Kontes Teflon valves. HF and the Lewis acids were handled in a stainless steel-Teflon-FEP vacuum system,[9] and solids, in the dry N_2 atmosphere of a glovebox. Vibrational spectra were recorded as previously described.[10]

Preparation of $H_2N_3^+AsF_6^-$. A prepassivated (with ClF_3 and HF) Teflon-FEP ampule that was closed by a stainless steel valve was loaded on the metal vacuum line with HF (4.6 g). On the Pyrex line, HN_3 (2.73 mmol) was added at -196 °C, and the mixture was homogenized at room temperature. AsF_5 (2.86 mmol) was added on the metal line at -196 °C, and the mixture was warmed to -78 °C for 1.5 h. The HF solvent and the unreacted starting material were pumped off while the ampule was warmed slowly to ambient temperature. Pumping was continued for 1 h at 20 °C. The ampule contained 633 mg of a white solid (weight calculated for 2.73 mmol of $H_2N_3^+AsF_6^-$ = 636 mg) which was identified by vibrational spectroscopy and X-ray diffraction as $H_2N_3^+AsF_6^-$.

Preparation of $H_2N_3^+SbF_6^-$. Antimony pentafluoride (2.74 mmol) was transferred on the metal line in a dynamic vacuum into a prepassivated Teflon-FEP U-tube that was kept at -78 °C and closed by two stainless steel valves. Anhydrous HF (1.6 g) was added at -196 °C, and the mixture was briefly warmed to room temperature. Hydrazoic acid (3.23 mmol) was added at -196 °C on the Pyrex line, and the mixture was warmed to room temperature. All material, volatile at room temperature, was pumped off for 30 min, resulting in a white, stable solid (760 mg; weight calculated for 2.74 mmol of $H_2N_3^+SbF_6^-$ = 766 mg) which was identified by vibrational spectroscopy and a crystal structure determination as $H_2N_3^+SbF_6^-$.

Preparation of $H_2N_3^+BF_4^-$. According to the procedure described above for $H_2N_3^+AsF_6^-$, HN_3 (2.88 mmol) was combined with BF_3 (3.23 mmol) in HF (5.66 g). Warming of the resulting mixture from -196 to -78 °C produced a gel-type product which on further warming to -22 °C formed a clear solution. Volatile products were pumped off at -22 °C for 2 h and at 20 °C for 10 min, leaving behind 379 mg of a white, somewhat tacky, solid (weight calculated for 2.88 mmol of $H_2N_3^+BF_4^-$ = 377 mg) which was identified by vibrational spectroscopy as $H_2N_3^+BF_4^-$.

† Dedicated to Professor G. Olah on the occasion of his 65th birthday.

(1) Rocketdyne.
(2) E. I. du Pont de Nemours and Company, Inc.
(3) University of California, Los Angeles.
(4) University of Southern California.
(5) Schmidt, A. *Chem. Ber.* **1966**, *99*, 2976.
(6) Mertens, A.; Lammertsma, K.; Arvanaghi, M.; Olah, G. A. *J. Am. Chem. Soc.* **1983**, *105*, 5657.
(7) Krakow, B.; Lord, R. C.; Neely, G. O. *J. Mol. Spectrosc.* **1968**, *27*, 198.
(8) Christe, K. O.; Wilson, W. W.; Schack, C. J. *J. Fluorine Chem.* **1978**, *11*, 71.
(9) Christe, K. O.; Wilson, R. D.; Schack, C. J. *Inorg. Synth.* **1986**, *24*, 3.
(10) Wilson, W. W.; Christe, K. O. *Inorg. Chem.* **1987**, *26*, 1573.

0002-7863/93/1515-1836$04.00/0 © 1993 American Chemical Society

Table I. Details of the Data Collection and Structure Refinement for $H_2N_3^+SbF_6^-$ at 20 K

formula	$H_2N_3SbF_6$
fw	279.78
cryst system	orthorhombic
space group	$Pmc2_1$
cryst dimens, mm	0.15 × 0.30 × 0.50
cryst color	colorless
cryst habit	irregular
a, Å	5.794 (3)
b, Å	5.113 (2)
c, Å	9.919 (5)
Z	2
V, Å^3	293.88
ρ(calcd), g/cm^3	1.79
radiation (λ, Å)	Mo Kα (0.7107)
abs coeff (μ), cm^{-1}	2.42
abs cor type	empirical
abs factor range (intensity)	1.14–1.00
F(000), e	154
temp, K	20
diffractometer	Huber (Crystal Logic)
scan mode; speed, deg/min	θ–2θ; 12.0
2θ range, deg	1–65
total no. of reflns measd	2095 ($+h,\pm k,\pm l$)
no. of unique reflns	649
R_{int}	0.024
no. of reflns used in refinement	587 ($I > 3\sigma(I)$)
no. of params refined	58
final shift/error: max, av	0.021, 0.002
max residual density, e/Å^3	1.55 (0.75 Å from Sb)
$R = \sum\|\|F_o\| - \|F_c\|\|/\sum\|F_o\|$	0.015
$R_w = (\sum w(\|F_o\| - \|F_c\|)^2/\sum w(\|F_o\|)^2)^{1/2}$	0.022
GOF = $(\sum w(\|F_o\| - \|F_c\|)^2/(N_o - N_v))^{1/2}$	1.024
isotropic extinction param (×10^5)	1.883

Crystal Structure Determination of $H_2N_3^+SbF_6^-$. Single crystals of $H_2N_3^+SbF_6^-$ were obtained by recrystallization from anhydrous HF solution. Suitable crystals were selected under a microscope inside the glovebox and sealed in quartz capillaries. Initial data collection was carried out at room temperature on a Siemens $P2_1$ diffractometer. The structure was solved and refined to an agreement factor of $R = 0.049$ for 409 reflections. This structure revealed an asymmetric $H_2N_3^+$ cation with two poorly-defined H atoms attached to one of the terminal N atoms. Since the hydrogen positions in this room-temperature X-ray analysis were not entirely satisfactory, it was decided to re-collect data at low temperature.

Low-temperature diffraction data were collected on a four-circle Huber diffractometer equipped with a closed-cycle helium refrigerator.[11] The crystal was slowly cooled, over a period of 4 h, to 20 (5) K. Accurate unit cell parameters at this temperature were obtained by least-squares refinement of 15 centered reflections and are listed in Table I together with other details of data collection and structure refinement. Intensity data at 20 K were collected with the θ–2θ step scan technique, up to a maximum 2θ of 65°. Three standard reflections measured after every 97 reflections showed no decay. A total of 2095 reflections were measured over one hemisphere of reciprocal space and were then averaged for multiple observations to give a set of 649 unique reflections. R(av) was 0.024. Corrections for Lorentz and polarization effects were made, and an empirical absorption correction was applied using the ψ-scan procedure.

The position of antimony was determined from a Patterson map, and the remaining non-hydrogen atom positions were obtained from the initial difference Fourier map. The structure was then refined using 587 reflections with $I > 3\sigma(I)$, first with isotropic and later with anisotropic thermal parameters. At this point, a difference electron density map revealed the positions of the hydrogen atoms at a distance of 0.85 Å from N(1). In the final cycles of least-squares refinement, the hydrogen atom positions were also refined with a fixed isotropic temperature factor. The assigned thermal parameter for the hydrogen atoms was 30% higher than the average isotropic thermal parameters of the rest of the atoms, excluding Sb. Refinement converged with final agreement factors of $R(F) = 0.015$ and $R_w(F) = 0.022$ and GOF = 1.024. In the final difference map, except for two ripples associated with Sb (1.55 and 1.51 e/Å^3 about 0.68 and 0.75 Å away, respectively), the maximum residual electron density was less than 0.75 e/Å^3. No significant correlations were observed. All data reduction, structure solution and refinement, and graphics were executed using the UCLA crystallographic package.[12]

(11) Strouse, C. E. *Rev. Sci. Instrum.* **1976**, *47*, 871–876.

Table II. Fractional Atomic Coordinates and Equivalent Isotropic Thermal Parameters (Å^2) with Esd's of the Refined Parameters in Parentheses for $H_2N_3^+SbF_6^-$ at 20 K

atom	x	y	z	10^4U_{eq}[a]
Sb	0.0000	0.13576 (3)	0.1873[b]	40 (1)
F(1)	−0.2303 (3)	−0.0176 (3)	0.0790 (2)	85 (6)
F(2)	0.2311 (3)	0.2909 (3)	0.2946 (2)	88 (6)
F(3)	0.0000	0.4289 (5)	0.0720 (3)	84 (10)
F(4)	0.0000	−0.1618 (5)	0.2993 (4)	83 (11)
N(1)	0.5000	−1.4511 (7)	1.0250 (4)	83 (14)
N(2)	0.5000	−1.6211 (6)	0.9282 (5)	85 (18)
N(3)	0.5000	−1.7781 (7)	0.8523 (4)	111 (15)
H(1)	0.388 (13)	−1.3753 (65)	1.020 (11)	127[c]

[a] $U_{eq} = [1/(6\pi^2)]\sum_i\sum_j\beta_{ij}\mathbf{a}_i\cdot\mathbf{a}_j$. [b] z coordinate held constant to define origin. [c] Assigned isotropic temperature factor held constant.

Table III. Interatomic Distances (Å) and Angles (deg) with Esd's in Parentheses for $H_2N_3^+SbF_6^-$ at 20 K[a]

		$H_2N_3^+$	
N(1)–N(2)	1.295 (5)	N(1)–H(1)	0.76 (7)
N(2)–N(3)	1.101 (6)	H(1)–H(1′)	1.30 (16)
N(1)–N(2)–N(3)	175.3 (5)	H(1)–N(1)–N(2)	107 (6)
H(1)–N(1)–H(1′)	118 (8)		
		SbF_6^-	
Sb–F(1)	1.884 (2)	Sb–F(3)	1.885 (3)
Sb–F(2)	1.885 (2)	Sb–F(4)	1.884 (3)
F(1)–Sb–F(1′)	90.20 (1)	F(2)–Sb–F(2′)	90.5 (1)
F(1)–Sb–F(2)	89.65 (8)	F(2)–Sb–F(3)	90.46 (8)
F(1)–Sb–F(2′)	179.58 (9)	F(2)–Sb–F(4)	90.4 (1)
F(1)–Sb–F(3)	89.15 (9)	F(3)–Sb–F(4)	178.8 (1)
F(1)–Sb–F(4)	90.00 (9)		

[a] Room-temperature parameters: N(1)–N(2) = 1.36 (5) Å, N(2)–N(3) = 1.06 (5) Å, N(1)–N(2)–N(3) = 173 (5)°.

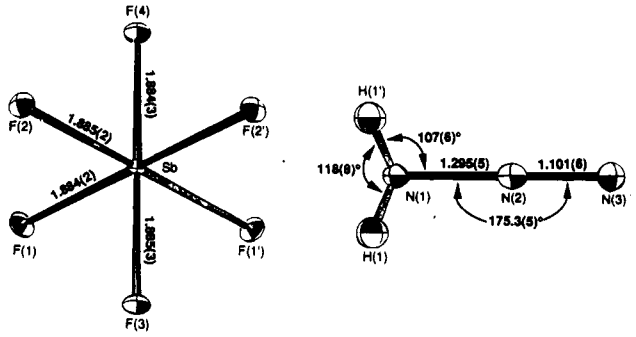

Figure 1. Atom numbering schemes, bond lengths (Å), and bond angles (deg) for $H_2N_3^+$ and SbF_6^- at 20 K.

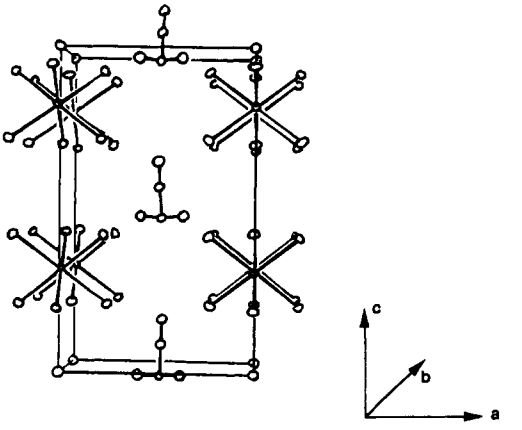

Figure 2. Packing diagram of $H_2N_3^+SbF_6^-$ viewed along the b axis.

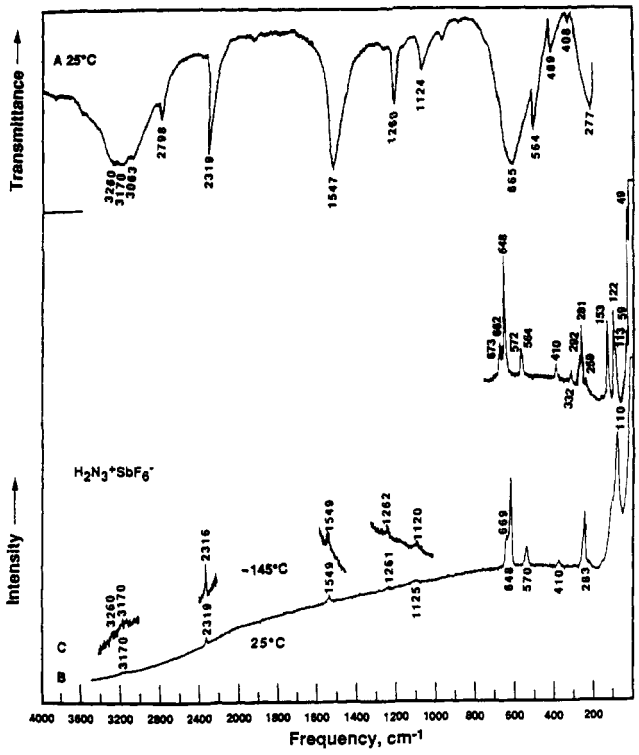

Figure 3. Vibrational spectra of solid $H_2N_3^+SbF_6^-$: trace A, infrared spectrum of a sample pressed between AgBr windows; traces B and C, Raman spectra recorded at 25 and −145 °C, respectively.

Final atomic coordinates with equivalent isotropic thermal parameters are listed in Table II. Interatomic distances and angles are given in Table III, and the anisotropic temperature factors are listed in Table 1S in the supplementary material. An Ortep plot of the molecule is shown in Figure 1, and unit cell packings along the *b* and *a* axes are shown in Figures 2 and 3, respectively.

Crystal Structure Determination of $H_2N_3^+AsF_6^-$. This compound crystallizes in the orthorhombic space group *Pma*2 (No. 28), with a = 20.056 Å, b = 5.468 Å, c = 5.523 Å, V = 604.7 Å^3, and Z = 4. Data were collected at room temperature, and the structure was refined to an agreement factor of R = 0.057 for 387 nonzero reflections. The structure shows a linear and apparently almost symmetric $H_2N_3^+$ cation [N–N = 1.16 (2) and 1.19 (2) Å; N–N–N = 177 (2)°]. However, the structure analysis was marred by extensive disordering of the AsF_6^- anion, and it is quite possible that the $H_2N_3^+$ cation suffers from a 2-fold packing disorder as well. The H atoms in $H_2N_3^+AsF_6^-$ could not be located.

Computational Methods. The geometry, vibrational frequencies, and force field of $H_2N_3^+$ were calculated, as previously described,[13] in the local density functional (LDF) approximation by using the program system DMol with a polarized double numerical basis set.

Results and Discussion

Syntheses and Properties of $H_2N_3^+$ Salts. Protonation of HN_3 by mixtures of HF and the strong Lewis acids SbF_5, AsF_5, and BF_3, followed by removal of solvent and unreacted starting material at room temperature, produces the $H_2N_3^+$ salts of SbF_6^-, AsF_6^-, and BF_4^-, respectively.

$$HN_3 + HF + XF_n \xrightarrow{HF} H_2N_3^+XF_{n+1}^-$$

Although the existence of the $H_2N_3^+$ cation in these solutions had previously been established by multinuclear NMR spectroscopy,[6] the actual salts had not been isolated and characterized. All salts are white, crystallinic solids that are stable at room temperature. They are strongly hygroscopic and, when exposed to moisture, form the corresponding H_3O^+ salts[14]

$$H_2N_3^+SbF_6^- + H_2O \rightarrow H_3O^+SbF_6^- + HN_3$$

as expected from H_2O being a stronger base than HN_3 and, therefore, being able to displace HN_3 from its salts.

X-ray Crystal Structure of $H_2N_3^+SbF_6^-$. The crystal structure of $H_2N_3^+SbF_6^-$ was determined both at room temperature and at 20 K. The structures were almost identical at both temperatures (see Table III and footnote), but the low-temperature data were of much better quality. The structure consists of well-separated $H_2N_3^+$ and SbF_6^- ions (see Figure 1). The SbF_6^- anion is a nearly perfect octahedron with angles ranging from 89.15 (9) to 90.5 (1)° and identical Sb–F bond lengths of 1.885 (3) Å. The $H_2N_3^+$ cation is asymmetric, with both hydrogens attached to the same nitrogen. Furthermore, the two N–N bond distances are very different, the N–N–N group is slightly distorted from linearity (N(1)–N(2)–N(3) = 175.3°), and the NH_2 group is pyramidal. These findings demonstrate that the structure of $H_2N_3^+$ is best described by I, with little contribution from resonance structure

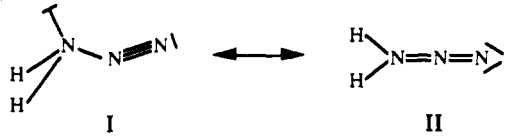

I II

II. The fact that the repulsion from the free valence electron pair on N(1) is larger than those from the two hydrogen ligands can account for N(2) being slightly bent away from this free pair. The observed N—N bond lengths are in good agreement with our expectations for an N—N single and an N≡N triple bond, and their differences are more pronounced than those found for other covalent azides such as CF_3N_3 (N(1)–N(2) = 1.252 (5) Å, N(2)–N(3) = 1.118 (3) Å)[15] or FN_3 (N(1)–N(2) = 1.253 (10) Å, N(2)–N(3) = 1.132 (10) Å).[16] The observed N–H bond length of 0.76 (7) Å is unrealistically short due to the fact that hydrogen does not possess any core electrons, and therefore, the X-rays are being diffracted by the binding electrons. This results in an artificially short N–H bond length, which is no surprise in view of the well-known difficulties of obtaining reliable hydrogen bond lengths by X-ray diffraction. On the basis of the ab initio calculation (see below), a realistic N–H bond distance in $H_2N_3^+$ is about 1.01 Å. The H–N–H and H–N–N bond angles, on the other hand, should not be affected, as the binding electrons are located along the N–H bond axes, and, therefore, are considered more reliable.

A packing diagram of $H_2N_3^+SbF_6^-$ is shown in Figure 2. The anion and the cation are located on crystallographic mirror planes. The anionic mirror plane passes through the atoms F(3)–Sb–F(4) whereas the cationic mirror plane passes through all three nitrogen atoms and bisects the H–N–H angle. The cations are stacked parallel to each other down the crystallographic *b* axis (see Figure 2) but are oriented perpendicular to each other in the *b*–*c* plane, causing a doubling of the repeat distance along the *c* axis. The nearest anion–cation interactions are N(1)···F(1) at 2.765 Å and H(1)···F(1) at 2.127 Å, which are significantly shorter than the

(12) The programs used in this work included modified versions of the following programs: REDUCE (Broach, Coppens, Becker, and Blessing), peak profile analysis, Lorentz and polarization corrections; ORFLS (Busing, Martin, and Levy), structure factor calculation, full-matrix least-squares refinement; ORFEE (Busing, Martin, and Levy), distance, angle, and error calculations; ORTEP (Johnson), figure plotting. Scattering factors and corrections for anomalous dispersion were taken from: *International Tables for X-ray Crystallography*; Kynoch Press; Birmingham, England, 1974; Vol. IV. All calculations were performed on a DEC VAX 3100 cluster.

(13) (a) Christe, K. O.; Wilson, R. D.; Wilson, W. W.; Bau, R.; Sukumar, S.; Dixon, D. A. *J. Am. Chem. Soc.* **1991**, *113*, 3795. (b) Dixon, D. A.; Andzelm, J.; Fitzgerald, G.; Wimmer, E.; Jasien, P. In *Density Functional Methods in Chemistry*; Labanowski, J., Andzelm, J., Eds.; Springer Verlag: New York, 1991; p 33. (c) Dixon, D. A.; Christe, K. O. *J. Phys. Chem.* **1992**, *96*, 1018. (d) Delley, B. *J. Chem. Phys.* **1990**, *92*, 508. Dmol is available commercially from BIOSYM Technologies, San Diego, CA. A FINE grid was used. The multipolar fitting functions for the model density used to evaluate the effective potential have angular momentum numbers of 3 for N and 2 for H.

(14) Christe, K. O.; Schack, C. J.; Wilson, R. D. *Inorg. Chem.* **1975**, *14*, 2224.

(15) Christe, K. O.; Christen, D.; Oberhammer, H.; Schack, C. J. *Inorg. Chem.* **1984**, *23*, 4283.

(16) Christen, D.; Mack, H. G.; Schatte, G.; Willner, H. *J. Am. Chem. Soc.* **1988**, *110*, 707.

Table IV. Calculated and Observed Geometries of Isoelectronic $H_2N_3^+$ and H_2NCN

	$[H_2N-N\equiv N]^+$			$H_2N-C\equiv N$			
	expt[a]	LDF	3-21G[b]	expt[c]	LDF	6-31G*[d]	STO-3G[d]
			Bond Distances, Å				
r_1, r_2 (N—H)	*e*	1.043	1.008	1.001	1.031	0.998	1.031
r_3 (N—X)	1.295 (5)	1.276	1.305	1.346	1.341	1.344	1.399
r_4 (X≡N)	1.101 (6)	1.126	1.088	1.160	1.172	1.138	1.158
			Bond Angles, deg				
α (H—N—H)	118 (8)	117.9	*f*	113.5	110.5	113.2	108.8
β_1, β_2 (H—N—X)	107 (6)	114.5	*f*	115.6	113.6	114.5	110.4
$\sum(\alpha+\beta_1+\beta_2)$[g]	332 (20)	346.9	360[f]	344.7	337.7	342.2	329.6
N—X≡N	175.3 (5)	175.2	*f*	[180][h]	176.1	178.2	176.7

[a] Data from crystal structure of $H_2N_3^+SbF_6^-$ at 20 K. [b] Data from ref 6. [c] Data from refs 24 and 30. [d] Data from ref 22. [e] The value of 0.76 (7) from Table III is much too short because of the shortcomings of X-ray diffraction methods for the determination of exact hydrogen bond distances and should not be used. [f] No angles were given in ref 6; however, from the stated planarity and C_{2v} symmetry of $H_2N_3^+$ $\sum(\alpha+\beta_1+\beta_2)$ must equal 360°. [g] This sum of the angles is a measure for the planarity of the NH_2 group, with 360° being planar and 328.5° being an ideal trigonal pyramid. [h] Assumed value.

Table V. Calculated and Observed Vibrational Frequencies (cm^{-1}) of Isoelectronic $H_2N_3^+$ and H_2NCN

Approx description of mode in point group C_s	Symmetry coodinates	$[H_2N-N\equiv N]^+$ obsd	$[H_2N-N\equiv N]^+$ calcd LDF	$[H_2N-N\equiv N]^+$ PED[a] LDF	$H_2N-C\equiv N$ obsd	$H_2N-C\equiv N$ calcd LDF	calcd 6-31G*[f]	calcd 4-31G*[g]	PED LDF	PED 4-31G*[g]
A' ν_1 ν sym NH_2	$S_1=\frac{1}{\sqrt{2}}(\Delta r_1+\Delta r_2)$	3170	3248	$98S_1+1S_3$	3420[b]	3375	3787	3722	$100S_1$	$100S_1$
ν_2 ν X≡N	$S_2=\Delta r_4$	2318	2350	$69S_2+31S_4$	2270[b]	2301		2611	$66S_2+34S_4$	$90S_2+14S_4$
ν_3 δ sciss NH2	$S_3=\frac{1}{\sqrt{6}}(2\Delta\alpha-\Delta\beta_1-\Delta\beta_2)$	1547	1526	$100S_3$	1595[b]	1556	1804	1818	$100S_3$	$102S_2$
ν_4 νN–X	$S_4=\Delta r_3$	1129	1190	$88S_4+8S_2+4S_6$	1055[b]	1092	1159	1170	$85S_4+8S_2+5S_3+2S_6$	$79S_4+10S_2$
ν_5 δNXN in plane	S_5 = N(–),X(+),N(–) in plane	530	516	$79S_5+20S_6$	(538)[d]	477	531	554	$85S_5+15S_6$	$74S_5+23S_6$
ν_6 δNH_2 wag (inversion at N)	$S_6=\frac{1}{\sqrt{3}}(\Delta\alpha+\Delta\beta_1+\Delta\beta_2)$	489	479	$72S_6+24S_5+3S_3$	$\binom{714,670}{414,364}$[e]	622	691	688	$86S_6+13S_5+1S_4$	$96S_6+27S_5+21S_4$
A" ν_7 vas NH_2	$S_7=\frac{1}{\sqrt{2}}(\Delta r_1-\Delta r_2)$	3280	3372	$98S_7+2S_8$	3480[b]	3469	3890	3829	$98S_7+1S_8$	$100S_7$
ν_8 δas NH_2	$S_8=\frac{1}{\sqrt{2}}(\Delta\beta_1-\Delta\beta_2)$	1259	1232	$99S_8+1S_9$	$\binom{1055}{\text{or } 1150}$[c]	1151	1323	1343	$98S_8+2S_9$	$93S_8$
ν_9 δNXN out of plane	$S_9=t_1+t_2$[h]	418	429	$85S_9+14S_8$	(437)[d]	408	463	485	$85S_9+15S_8$	$99S_9$

(a) in percent; (b) infrared gas phase frequencies from ref. 21; (c) see text; (d) Raman of the liquid (ref. 28) and solid (ref. 32); (e) components of the inversion splitting (see refs. 21,24,27); (f) data from ref. 22; (g) data from ref 24; (h) t_1 = angle of C(2)–N(3) with respect to the plane H(1)–C(2)–N(1); t_2 = angle of C(2)–N(3) with respect to the plane H(2)–C(2)–N(1); see also comments made in the discussion of the results of the normal coordinate analysis.

sums of their Pauling van der Waals radii.[17] Although these short distances suggest appreciable hydrogen–fluorine bridging, they do not result in a significant distortion of the SbF_6^- octahedron (see above).

The above crystal structure demonstrates that $H_2N_3^+$ has indeed the asymmetric aminodiazonium structure. This is not surprising in view of a previous ab initio calculation which indicated that the aminodiazonium structure is 49.8 kcal mol^{-1} more favorable than the symmetric diazenium structure.[6] It must be pointed out, however, that, in spite of the good agreement between the predicted[6] and our observed N–N bond lengths (1.305 and 1.088 Å versus 1.295 (5) and 1.101 (6) Å), the previous calculation[6] predicted a planar NH_2 group whereas the crystal structure and our LDF calculations (see below) show that the NH_2 group in $H_2N_3^+$ is pyramidal. This was due to the lack of polarization functions on the nitrogens at the 3-21G level.

Computational Results. To support our analysis of the vibrational spectra of the $H_2N_3^+$ cation, the structure, vibrational frequencies, and force field of the free $H_2N_3^+$ cation in the gas phase were calculated using local density functional (LDF) theory. To test the quality of these computations, the electronic structure of the known,[18-32] isoelectronic cyanamide molecule, H_2NCN, was also calculated. The results are summarized in Tables IV–VI and demonstrate that, for this type of molecule, LDF theory duplicates

Table VI. Symmetry Force Constants (mdyn/Å) of $H_2N_3^+$ and H_2NCN Calculated by the LDF Method

$H_2N_3^+$

A'	1	2	3	4	5	6	A"	7	8	9
1	6.04	-0.20	0.01	0.24	0.02	0.25	7	6.11	0.08	0.04
2		20.17	0.01	0.57	0.06	-0.20	8		0.74	-0.11
3			0.54	-0.47	-0.03	-0.14	9			1.94
4				9.53	0.18	0.99				
5					0.56	-0.14				
6						0.54				

H_2NCN

A'	1	2	3	4	5	6	A"	7	8	9
1	6.48	-0.14	0.07	0.18	0.04	0.32	7	6.53	0.17	-0.02
2		17.58	-0.01	0.39	0.04	-0.11	8		0.64	-0.13
3			0.57	-0.33	-0.03	-0.03	9			1.04
4				7.98	0.09	0.65				
5					0.51	-0.03				
6						0.45				

(17) Pauling, L. *The Nature of the Chemical Bond*, 3rd ed.; Cornell University Press: Ithaca, NY, **1960**; p 260.

(18) Brown, R. D.; Godfrey, P. D.; Head-Gordon, M.; Wiedenmann, K. H.; Kleibömer, B. *J. Mol. Spectrosc.* **1988**, *130*, 213.

(19) Hunt, R. D.; Andrews, L. *J. Phys. Chem.* **1987**, *91*, 2751.

(20) Read, W. G.; Cohen, E. A.; Picket, H. M. *J. Mol. Spectrosc.* **1986**, *115*, 316.

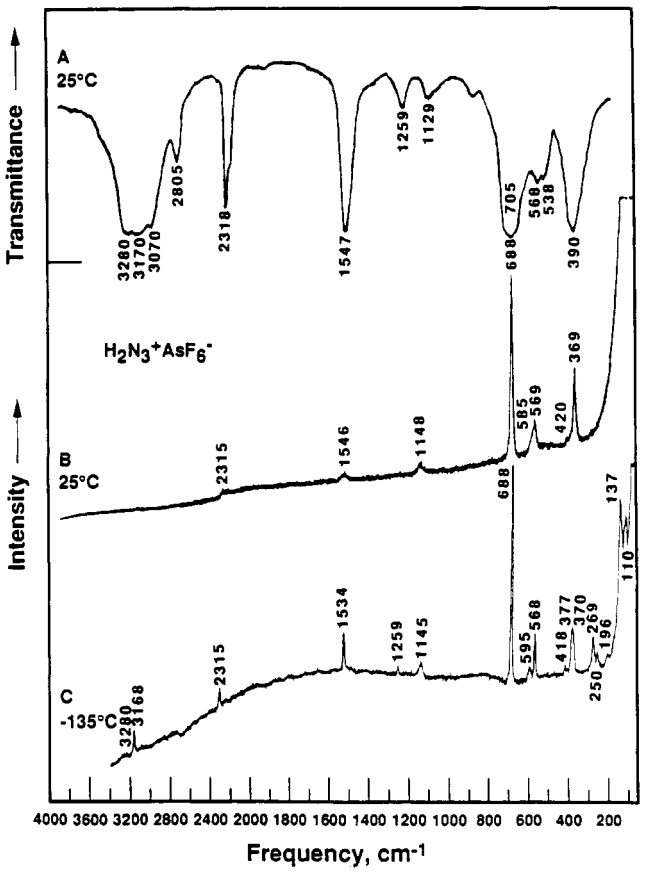

Figure 4. Vibrational spectra of solid $H_2N_3^+AsF_6^-$: trace A, infrared spectrum of a sample pressed between AgBr windows; traces B and C, Raman spectra recorded at 25 and −135 °C, respectively.

the experimental frequency values better than calculations at either the 4-31G* [24] or 6-31G* [22] level. In agreement with previous calculations at the 4-31G[24] or higher levels[22] for H_2NCN, the lowest energy structure found for $H_2N_3^+$ by using LDF theory is nonplanar (C_s symmetry) with a pyramidal amino group. The planar C_{2v} structure previously calculated for $H_2N_3^+$ at the 3-21G level[6] is due to the lower level of theory used and, for isoelectronic H_2NCN, represents a saddle point on the potential energy surface.[22] It should also be pointed out that LDF theory predicts the H_2N–N group in $H_2N_3^+$ to be considerably flatter than the H_2N–C group in H_2NCN. This should result in a lower inversion barrier for the NH_2 group in $H_2N_3^+$, which is also apparent from the lowering of the frequency of the NH_2 wagging mode, $\nu_6(A')$, which, on the basis of its symmetry coordinate and potential energy distribution, represents the inversion motion (see below).

Vibrational Spectra. Infrared and Raman spectra were recorded for $H_2N_3^+SbF_6^-$, $H_2N_3^+AsF_6^-$, and $H_2N_3^+BF_4^-$ (see Figures 3–5). Table VII shows the observed frequencies and their assignments.

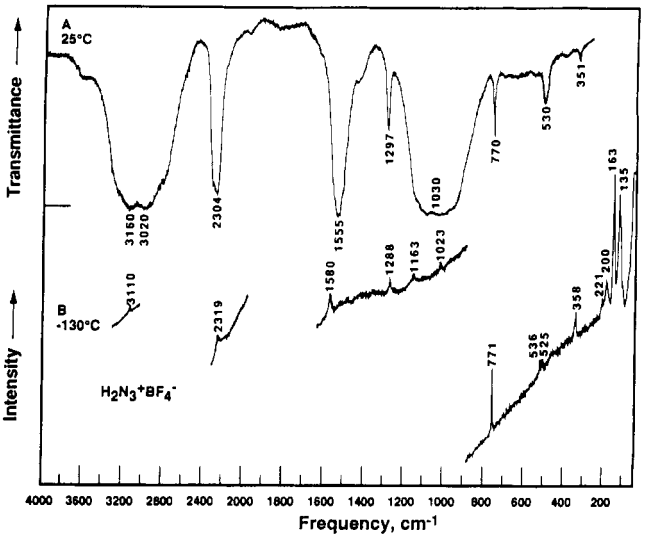

Figure 5. Vibrational spectra of solid $H_2N_3^+BF_4^-$: trace A, infrared spectrum of a sample pressed between AgBr windows; trace B, Raman spectra recorded at −130 °C.

Approximate mode descriptions, symmetry coordinates, and potential energy distributions for $H_2N_3^+$ and isoelectronic H_2NCN are included in Table V. The LDF force fields for $H_2N_3^+$ and H_2NCN were analyzed in terms of internal coordinates and are given in Table VI.

Although cyanamide, H_2NCN, is a simple molecule of great industrial importance and its structure is well-known from microwave spectroscopy,[20,30,31] its vibrational analysis is still incomplete. This is partially due to experimental difficulties, i.e. its low vapor pressure and tendency to polymerize, and to complications caused by its low inversion barrier at the nitrogen atom.

The H_2NCN molecule and the isoelectronic $H_2N_3^+$ cation possess symmetry C_s, and their nine fundamental vibrations are classified as $\Gamma = 6A' + 3A''$ (see Table V). Of the nine fundamental vibrations of H_2NCN, the antisymmetric NH_2 deformation, $\nu_8(A'')$, has not been experimentally observed, the two NCN bending modes, $\nu_5(A')$ and $\nu_9(A'')$, have been observed only in the liquid phase[28] or solution,[24] and the NH_2 wagging mode, $\nu_6(A')$, is complicated by inversion splittings.[21] Nevertheless, H_2NCN served as a good case for testing the accuracy of the LDF calculations. As can be seen from Table V, our LDF results for H_2NCN are in good agreement with the experimental frequencies. Consequently, the LDF values for $H_2N_3^+$ should be equally good and were used as a guide for the following assignments for $H_2N_3^+$.

The assignment of the two NH_2 stretching modes, $\nu_1(A')$ and $\nu_7(A'')$, the N≡N stretching mode, $\nu_2(A')$, and the NH_2 scissoring mode, $\nu_3(A')$, to the bands at about 3170, 3280, 2318, and 1547 cm^{-1}, respectively, is unambiguous. In the 1100–1300-cm^{-1} region, two bands are observed at about 1129 and 1259 cm^{-1}, respectively, which, on the basis of the LDF predictions, should represent the N–N stretching mode, $\nu_4(A')$, and the antisymmetric NH_2 deformation, $\nu_8(A'')$, respectively. This choice of assignments is also supported by the observations that the 1259-cm^{-1} mode is more intense in the infrared and less intense in the Raman spectra and that, in the room-temperature Raman spectrum of $H_2N_3^+SbF_6^-$, it is broadened so much that it is no longer observable. A similar broadening of the Raman bands at ambient temperature has also been observed for the remaining NH_2-group modes in the $H_2N_3^+SbF_6^-$ spectrum. This positive identification of the antisymmetric NH_2 deformation vibration for $H_2N_3^+$ suggests that, in H_2NCN, this mode should occur in a similar frequency range and might either by assigned to the broad band at about 1150 cm^{-1} in the infrared spectrum of liquid H_2NCN,[27] or, in the gas phase, coincide with the N–C stretching mode at 1055 cm^{-1}.

The remaining three, yet unassigned, fundamental vibrations are the NH_2 wagging mode, $\nu_6(A')$, and the two N_3 skeletal deformation modes, $\nu_5(A')$ and $\nu_9(A'')$. On the basis of the LDF calculations, these three modes are expected to occur in the

(21) Birk, M.; Winnewisser, M. *Chem. Phys. Lett.* **1986**, *123*, 382.
(22) Saebo, S.; Farnell, L.; Riggs, N. V.; Radom, L. *J. Am. Chem. Soc.* **1984**, *106*, 5047.
(23) Khaikin, L. S.; Mochalov, V. I.; Grikina, O. E.; Pentin, Yu. A. *Vestn. Mosk. Univ., Ser. 2: Khim.* **1983**, *24*, 536.
(24) Ichikawa, K.; Hamada, Y.; Sugawara, Y.; Tsuboi, M.; Kato, S.; Morokuma, K. *Chem. Phys.* **1982**, *72*, 301.
(25) Daoudi, A.; Pouchan, C.; Sauvaitre, H. *J. Mol. Struct.* **1982**, *89*, 103.
(26) King, S. T.; Strope, J. H. *J. Chem. Phys.* **1971**, *54*, 1289.
(27) Jones, T. R.; Sheppard, N. *J. Chem. Soc. D* **1970**, 715.
(28) Fletcher, W. H.; Brown, F. B. *J. Chem. Phys.* **1963**, *39*, 2478.
(29) Wagner, G. D.; Wagner, E. L. *J. Chem. Phys.* **1960**, *34*, 1480.
(30) Tyler, J. K.; Sheridan, J.; Costain, C. C. *J. Mol. Spectrosc.* **1972**, *43*, 248.
(31) Johnson, D. R.; Suenram, R. D.; Lafferty, W. J. *Astrophys. J.* **1976**, *208*, 245.
(32) Durig, J. R.; Walker, M.; Baglin, F. G. *J. Chem. Phys.* **1968**, *48*, 4675.

Table VII. Vibrational Spectra for Solid $H_2N_3^+SbF_6^-$, $H_2N_3^+AsF_6^-$, and $H_2N_3^+BF_4^-$ and Their Assignments

obsd freq, cm^{-1} (rel intens)										
$H_2N_3^+SbF_6^-$			$H_2N_3^+AsF_6^-$			$H_2N_3^+BF_4^-$				
IR	Raman		IR	Raman		IR	Raman	assignt (point group)		
25 °C	25 °C	−144 °C	25 °C	25 °C	−135 °C	25 °C	−130 °C	$H_2N_3^+$ (C_s)	XF_6^- (O_h)	BF_4^- (T_d)
3260 vs		3260 (0+)	3280 vs		3280 (0+)	3160 vs		$\nu_7(A'')$		
3170 vs	3170 (0+)	3170 (0.5)	3170 vs		3168 (0.9)	3020 vs	3110 (0.2)	$\nu_1(A')$		
3063 m			3070 m					$2\nu_3(A')$		
2798 m			2805 m			2850 sh		$(\nu_3 + \nu_8)(A'')$		
2319 s	2319 (0.7)	2316 (2)	2318 s	2315 (0.3)	2315 (0.7)	2304 s	2319 (0.7)	$\nu_2(A')$		
1958 vw			1960 vw			1995 vw		$(\nu_3 + \nu_9)(A'')$		
1547 vs	1549 (0.8)	1549 (0.6)	1547 vs	1546 (0.4)	1534 (1.6)	1555 vs	1580 (1.5)	$\nu_3(A')$		
1310 vw			1400 vw						$(\nu_1 + \nu_3)(F_{1u})$	
1260 m	1261 (0.4)	1262 (0.4)	1259 m		1259 (0.4)	1297 m	1288 (1)	$\nu_8(A'')$		$(\nu_1 + \nu_4)(F_2)$
1220 vw									$(\nu_2 + \nu_3)(F_{1u} + F_{2u})$	
1124 mw	1125 (0.5)	1120 (0.5)	1129 mw	1148 (0.5)	1145 (0.7)		1163 (0.5)	$\nu_4(A')$		
						1030 vs	1023 (0.2)			$\nu_3(F_2)$
1025 vw								$(\nu_5 + \nu_6)(A')$		
						770 mw	771 (4.8)			$\nu_1(A_1)$
665 vs	669 (3)	673 (2), 662 (1)	705 vs						$\nu_3(F_{1u})$	
	648 (10)	648 (10)		688 (10)	688 (10)				$\nu_1(A_{1g})$	
	570 (2.3)	572 (2.4)		585 sh	595 (0.5)					
564 m		564 (1)	568 m	569 (1.6)	568 (2)				$\nu_2(E_g)$	
530 sh			538 m			530 mw	536 (0.5), 525 (0.5)	$\nu_5(A')$		$\nu_4(F_2)$
489 mw								$\nu_6(A')$		
408 vw	410 (0.8)	410 (1.0)		420 sh	418 (0.3)	420 m		$\nu_9(A'')$		
277 s			390 s						$\nu_4(F_{1u})$	
		332 (0.8)						F···H bridge		
		292 (2)			377 (1.9)					
	283 (6.2)	281 (5.8)		369 (4)	370 (1.7)				$\nu_5(F_{2g})$	
		259 (0.5)						F···H bridge		
						351 w	358 (1.9)			$\nu_2(E)$
					269 (1.5), 250 (0.5)				$\nu_6(F_{2u})$	
	150 sh	153 (8)			196 (0.2)		221 (0.5)			
	110 (10)	122 (8.5)			137 (4)		200 (2)		lattice vibrations	
		113 (2)			110 (3.5)		163 (10)			
		59 (2)					135 (8)			
		49 (8)								

400–500-cm^{-1} frequency range, which is complicated by bands due to the anions. Futhermore, the A″ skeletal bending mode, ν_9, is expected to be of very low infrared intensity,[23] and the NH_2 wagging mode, $\nu_6(A')$, should not exhibit any inversion splittings since in the crystallinic salts the hydrogens are locked into fixed positions by fluorine bridges (see X-ray crystal structure section).

Inspection of the low-temperature Raman spectra of $H_2N_3^+SbF_6^-$ and $H_2N_3^+AsF_6^-$ reveals a reasonably intense band at 410–420 cm^{-1}, which has a very weak counterpart in the infrared spectra and is only slightly broadened at room temperature. Hence, this vibration should belong to one of two skeletal bending modes of $H_2N_3^+$. Since, in the Raman spectra of liquid[24,28] or dissolved[24] H_2NCN, the out-of-plane NCN deformation mode has by far the highest intensity of the three modes in question and the 410–420-cm^{-1} frequency value is very close to that of 429 cm^{-1} calculated by us for the out-of-plane N_3 deformation mode of $H_2N_3^+$, this 410–420-cm^{-1} band can be assigned with confidence to the $\nu_9(A'')$ mode of $H_2N_3^+$.

The two remaining A′ modes, ν_5 and ν_6, are more difficult to assign. In view of their similar predicted frequencies (530 and 489 cm^{-1}) and related motions, we expect their symmetry coordinates to be strongly mixed (see PED of Table V), i.e. to be symmetric and antisymmetric combinations of S_5 and S_6. Both modes are expected to be of low Raman[32] but significant infrared intensity[24] and, therefore, should be detectable in the infrared spectra. The infrared spectrum of $H_2N_3^+SbF_6^-$ shows a shoulder at 530 cm^{-1} and a medium weak band at 489 cm^{-1}, and that of $H_2N_3^+AsF_6^-$ shows a medium band at 538 cm^{-1}. In $H_2N_3^+BF_4^-$, the 530-cm^{-1} region is obscured by the antisymmetric BF_4^- deformation, $\nu_4(F_2)$. Consequently, the ν_5 and ν_6 modes of $H_2N_3^+$ are tentatively assigned to the bands at about 530 and 489 cm^{-1}, respectively.

The above assignments can account for all the observed features in the vibrational spectra of the $H_2N_3^+$ salts, except for a medium weak band at 900 cm^{-1} and a shoulder at 820 cm^{-1} in the infrared spectrum of $H_2N_3^+AsF_6^-$. These two features are of variable intensity and show no counterparts in the IR spectrum of $H_2N_3^+SbF_6^-$. Therefore, they are judged to be due to an unknown impurity.

In the low-temperature Raman spectra of $H_2N_3^+SbF_6^-$ and $H_2N_3^+AsF_6^-$, the anion bands become much more complex than those in the room-temperature spectra. This is attributed to the freezing out of ion rotation, which for the anions causes splittings into degenerate components and violations of the O_h selection rules, as shown by the observation of the ν_6 mode for AsF_6^-. In addition, the low-temperature Raman spectrum of $H_2N_3^+SbF_6^-$ shows two bands at 332 and 259 cm^{-1}, which probably are not due to the SbF_6^- anion but represent H···F bridge bonds. This temperature effect on the vibrational spectra might also cause a significant broadening of the NH_2 wagging band, ν_6, at room temperature and, thereby, contribute to the difficulty of observing this mode in our infrared spectra.

In summary, the nine fundamental vibrations of $H_2N_3^+$ have been observed with frequencies which are in very good agreement with our LDF calculations. This confirms the asymmetric nonplanar aminodiazonium structure of $H_2N_3^+$, found by the X-ray crystal structure determination. The previous failure[5] to observe most of these bands for $H_2N_3^+SbCl_6^-$ is attributed to their relatively low infrared intensities and relative broadness at room temperature.

Normal-Coordinate Analysis. To support our vibrational assignments for $H_2N_3^+$, normal-coordinate analyses were carried out for $H_2N_3^+$ and isoelectronic H_2NCN (see Tables V and VI) with the LDF force fields. The corresponding frequencies and

symmetry coordinates are listed in Table V. Our LDF force field for H_2NCN is in good general agreement with that previously published[24] by Ichikawa et al. at the 4-31G* level of theory, if it is kept in mind that the frequencies at the 4-31G* level are on average about 10% higher than the experimental ones. The potential energy distributions are given in Table V and support the given mode descriptions.

A special comment is required on the magnitudes of F_{99} in our force fields, which are given in Table VI. The listed F_{99} values are clearly too high and should be comparable to those of F_{55}. The $\nu_5(A')$ and $\nu_9(A'')$ modes represent the in-plane and out-of-plane deformations of the nearly linear NXN groups, which, therefore, should be almost degenerate and exhibit similar frequencies and force constants. Whereas the frequencies of ν_9 are comparable to those of ν_5, the F_{99} values in Table VI are about 2-4 times larger than those of F_{55}. This is an artifact caused by the inability to exactly describe with our computer input code the S_9 symmetry coordinate of the out-of-plane NXN deformation for these molecules when they possess a slightly bent NXN group. Our program to convert the Cartesian second derivatives to symmetry-adapted internal coordinates allows for only four kinds of internal motions: bond stretching, angle bending, a dihedral angle between two planes, and the minimum angle that a bond forms with a plane. Thus, the $\nu_9(A'')$ mode had to be defined as the sum of the angles formed between the X-N(2) bond and the two planes defined by H(1)N(1)X and H(2)N(1)X. By making the NXN bonds linear, we were able to properly describe S_9 with this code and obtain values for F_{99} ($H_2N_3^+$, 0.47 mdyn/Å; H_2N-CN, 0.44 mdyn/Å) that are in excellent agreement with our expectations (see above) and those previously reported.[24] The PED ($94S_9 + 6S_8$) for the revised F_{99} values was similar to those given in Table V, while the remainder of the A'' force field remained practically unchanged.

Acknowledgment. The authors thank Dr. C. J. Schack and Mr. R. D. Wilson for their help, Dr. R. Minkwitz for bringing his unpublished studies on $H_2N_3^+SbCl_6^-$ to our attention, and the U.S. Army Research Office and the U.S. Air Force Phillips Laboratory for financial support of the work at Rocketdyne. T.M. thanks the Deutsche Forschungs Gemeinschaft for the provision of a postdoctoral fellowship.

Supplementary Material Available: Table 1S, listing anisotropic temperature factors (1 page); Table 2S, listing observed and calculated structure factors (3 pages). Ordering information is given on any current masthead page.

The Vanadium(IV) Enterobactin Complex: Structural, Spectroscopic, and Electrochemical Characterization[1]

Timothy B. Karpishin, Torin M. Dewey, and Kenneth N. Raymond*

Contribution from the Department of Chemistry, University of California, Berkeley, California 94720. *Received August 24, 1992*

Abstract: The siderophore enterobactin (H_6ent) has been crystallized as the vanadium(IV) complex in the compound K_2[V(ent)]·3DMF from dimethylformamide (DMF) solution. The pseudooctahedral coordination of the metal ion is through the three catechol groups and has approximate C_3 molecular point symmetry. The geometry is intermediate between trigonal prismatic and octahedral, with a twist angle of 28°. For comparison, the unconstrained complex of *N*-ethyl-2,3-dihydroxybenzamide (H_2eba) has been determined. The twist angle in $[V(eba)_3]^{2-}$ is 36°, somewhat larger than in the constrained enterobactin complex. The other metrical parameters are essentially identical between the two. Both the stability and the Δ chirality of the enterobactin complex are explained as due to the conformation of the triserine backbone. Molecular modeling calculations correctly predict this chiral preference as well as that for the complex of the (linear trimer) enterobactin hydrolysis product. The V-O bond distances in $[V(ent)]^{2-}$ average 1.946(7) and 1.939(5) Å to the ortho and meta catechol oxygens, respectively. Hydrogen bonding between the amide proton and the ortho catechol oxygen is an important feature of the structure. Comparison of the conformation of the trilactone serine ring in the vanadium enterobactin complex with two related trilactones shows that the conformation seen is characteristic of this triserine structure and is not a result of the metal complexation or of hydrogen bonding within the triserine ring. This also implies that the free ligand has a conformation similar to that seen in the metal complex. The potassium cations are partially coordinated by the meta catechol oxygens. Molecular modeling indicates that a smaller cation such as calcium cannot fit in the cavity formed between the octahedral catechol coordination site and the triserine ring. The UV/vis spectrum of $[V(ent)]^{2-}$ has been assigned on the basis of earlier quantitative spectroscopic studies. The spectroscopic parameters indicate that the M-O bonding is stronger in the vanadium complex than in the iron complex of enterobactin, partially due to strong π bonding. A quasi reversible reduction potential (in DMF vs SCE) is found for the V^V/V^{IV} couple of +0.39 V. For K_2[V(ent)]·3DMF, space group $P2_1$, a = 13.164(3), b = 10.001(1), c = 16.600(2) Å, β = 93.96°, z = 2, V = 2180(1) Å^3. For 5551 unique data with $F_o^2 > 3\sigma(F_o^2)$ R = 0.049, R_w = 0.062. For K_2[V(eba)$_3$]·3DMF, space group $Pa\bar{3}$, a = 20.632(5) Å, z = 8, V = 8783(5) Å^3. For 2526 unique data with $F_o^2 > 3\sigma(F_o^2)$ R = 0.051, R_w = 0.058.

Introduction

Most aerobic and anaerobic bacteria synthesize and excrete low molecular weight compounds (siderophores) for the solubilization and transport of iron.[2-4] Since the iron supply is often a limiting factor in the growth of these microbes, siderophores and their corresponding transport systems play an important role in bacterial virulence.[5] Of the approximately 200 siderophores now discovered, enterobactin (Figure 1), produced by enteric bacteria such as *Escherichia coli*, has received considerable attention. Since its discovery in 1970,[6,7] the synthesis,[8-10] biosynthesis,[11] microbial transport,[5,12-14] and solution thermodynamics[15-17]

* To whom correspondence should be addressed.

(1) Paper number 49 in the series Coordination Chemistry of Microbial Iron Transport. The previous paper (number 48) in this series: Abu-Dari, K.; Raymond, K. N. *J. Coord. Chem.* **1992**, *26*, 1-14. [Note that the series number cited in that article is incorrect. Papers 47 and 46 in the series are ref 31 and 28 of this paper, respectively.]

(2) Matzanke, B. F.; Müller-Matzanke, G.; Raymond, K. N. In *Iron Carriers and Iron* Proteins; Loehr, T. M., Ed.; VCH Publishers: New York, 1989; p. 1.

(3) Raymond, K. N.; Müller, G.; Matzanke, B. F. *Top. Curr. Chem.* **1984**, *123*, 49.

0002-7863/93/1515-1842$04.00/0 © 1993 American Chemical Society